Baryon number and electric charge fluctuations in Pb+Pb collisions at relativistic energies

V. P. Konchakovski,[1,2,3] M. I. Gorenstein,[1,3] E. L. Bratkovskaya,[3] and H. Stöcker[3,4]
[1]*Bogolyubov Institute for Theoretical Physics, Kiev, Ukraine*
[2]*Shevchenko National University, Kiev, Ukraine*
[3]*Frankfurt Institute for Advanced Studies, Frankfurt, Germany*
[4]*Institut für Theoretische Physik, Johann Wolfgang Goethe Universität, Frankfurt, Germany*
(Received 22 June 2006; published 21 December 2006)

Event-by-event fluctuations of the net baryon number and electric charge in nucleus-nucleus collisions are studied in Pb+Pb at SPS energies within the Hadron-String Dynamics (HSD) transport model. We reveal an important role of the fluctuations in the number of target nucleon participants. They strongly influence all measured fluctuations even in the samples of events with rather rigid centrality trigger. This fact can be used to check different scenarios of nucleus-nucleus collisions by measuring the multiplicity fluctuations as a function of collision centrality in fixed kinematical regions of the projectile and target hemispheres. The HSD results for the event-by-event fluctuations of electric charge in central collisions at 20A, 30A, 40A, 80A, and 158A GeV are in a good agreement with the NA49 experimental data and considerably larger than expected in a quark-gluon plasma. This demonstrates that the distortions of the initial fluctuations by the hadronization phase and, in particular, by the final resonance decays dominate the observable fluctuations.

DOI: 10.1103/PhysRevC.74.064911 PACS number(s): 25.75.Gz, 24.60.−k

I. INTRODUCTION

The aim of the present article is to study the fluctuations of the net baryon number and electric charge in nucleus-nucleus ($A + A$) collisions at energies at Super-Proton-Synchrotron (SPS) of 20, 30, 40, 80, and 150A GeV. We use the HSD [1] transport approach which reproduces both the different particle multiplicities and longitudinal differential rapidity distributions for central collisions of Au+Au (or Pb+Pb) from AGS to SPS energies rather well [2]. The fluctuation in High energy nuclear collisions (see, e.g., Refs. [3–12] and references therein) reveal a new physical information. The fluctuations in $A + A$ collisions are studied on an event-by-event basis: a given observable is measured in each event and the fluctuations are evaluated for a specially selected set of these events. We recall that the statistical model has been successfully used to describe the data on hadron multiplicities in relativistic $A + A$ collisions (see, e.g., Ref. [13] and a recent review [14]) as well as in elementary particle collisions [15]. This gives rise to the question whether the fluctuations, in particular the multiplicity fluctuations, do also follow the statistical hadron-resonance gas results. Recently the particle number fluctuations have been studied in different statistical ensembles [16]; the statistical fluctuations can be closely related to phase transitions in QCD matter, with specific signatures for 1st and 2nd order phase transitions as well as for the critical point [6,7].

In addition to the statistical fluctuations the complicated time evolution of $A + A$ collisions generates *dynamical* fluctuations. The fluctuations in the initial energy deposited inelastically in the statistical system yield *dynamical* fluctuations of all macroscopic parameters, like the total entropy or strangeness content. The observable consequences of the initial energy density fluctuations are sensitive to the equation of state and can therefore be useful as signals for phase transitions [12]. Even when the data are obtained with a centrality trigger the number of nucleons participating in inelastic collisions still fluctuates considerably. In the language of statistical mechanics, these fluctuations in the participant nucleon number correspond to volume fluctuations. Secondary particle multiplicities scale linearly with the volume; hence, volume fluctuations translate directly to particle number fluctuations.

The present work is a continuation of our recent study [17] where we analyzed the charged particle number fluctuations in Pb+Pb collisions at 158A GeV within the Ultra-relativistic Quantum Molecular Dynamics (UrQMD) and HSD transport approaches. The net baryon number and electric charge event-by-event fluctuations are studied in different rapidity regions of the projectile and target hemispheres.

The article is organized as follows. Section II presents the HSD results for the fluctuations of the number of nucleon participants while Secs. III and IV give the net baryon number fluctuations and electric charge fluctuations, respectively. In Sec. V we discuss the fluctuations in the samples of most central collisions, Sec. VI shows a comparison of our calculations with experimental data from the NA49 Collaboration, and Sec. VII finally concludes the present study.

II. FLUCTUATIONS OF THE NUMBER OF PARTICIPANTS

In each $A + A$ collision only a fraction of all $2A$ nucleons interact. These are called participant nucleons and are denoted as $N_P^{\rm proj}$ and $N_P^{\rm targ}$ for the projectile and target nuclei, respectively. The nucleons, which do not interact, are called the projectile and target spectators, $N_S^{\rm proj} = A - N_P^{\rm proj}$ and $N_S^{\rm targ} = A - N_P^{\rm targ}$. The fluctuations in high energy $A + A$ collisions are dominated by a geometrical variation of the impact parameter. However, even for the fixed impact parameter the number of participants, $N_P \equiv N_P^{\rm proj} + N_P^{\rm targ}$, fluctuates from

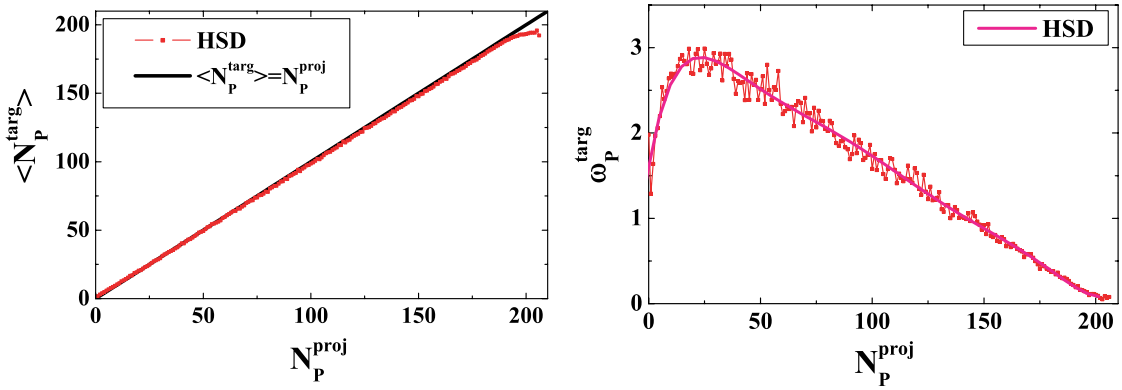

FIG. 1. (Color online) The HSD simulations in Pb+Pb collisions at 158A GeV for the average value $\langle N_P^{\rm targ}\rangle$ (left) and the scaled variances $\omega_P^{\rm targ}$ (right) as functions of $N_P^{\rm proj}$.

event to event. This is because of the fluctuations of the initial states of the colliding nuclei and the probabilistic character of the interaction process. The fluctuations of N_P form usually a large and uninteresting background. To minimize its contribution the NA49 Collaboration has selected samples of collisions with a fixed number of projectile participants. This selection is possible because of a measurement of $N_S^{\rm proj}$ in each individual collision by a calorimeter that covers the projectile fragmentation domain. However, even in the samples with $N_P^{\rm proj} = {\rm const}$ the number of target participants fluctuates considerably. Hence, an asymmetry between projectile and target participants is introduced; i.e., $N_P^{\rm proj}$ is constant by constraint, whereas $N_P^{\rm targ}$ fluctuates independently.

In the following, the variance, ${\rm Var}(n) \equiv \langle n^2\rangle - \langle n\rangle^2$, and scaled variance, $\omega_n \equiv {\rm Var}(n)/\langle n\rangle$, where n stands for a given random variable and $\langle\cdots\rangle$ for event-by-event averaging, will be used to quantify fluctuations. In each sample with $N_P^{\rm proj} = {\rm const}$, the number of target participants fluctuates around its mean value, $\langle N_P^{\rm targ}\rangle$, with the scaled variance $\omega_P^{\rm targ}$. From an output of the HSD minimum bias simulations of Pb+Pb collisions at 158A GeV we form the samples of events with fixed values of $N_P^{\rm proj}$. Figure 1 presents the HSD average value $\langle N_P^{\rm targ}\rangle$ (left) and the scaled variances $\omega_P^{\rm targ}$ (right) as functions of $N_P^{\rm proj}$. One finds $\langle N_P^{\rm targ}\rangle \simeq N_P^{\rm proj}$; the deviations are only seen at very small ($N_P^{\rm proj} \approx 1$) and very large ($N_P^{\rm proj} \approx A$) numbers of projectile participants. The fluctuations of $N_P^{\rm targ}$ are quite strong: $\omega_P^{\rm targ} > 2$ at $N_P^{\rm proj} = 10$–80.

The consequences of the asymmetry between projectile and target hemispheres depend on the $A + A$ dynamics. According to Ref. [18] different models of hadron production in relativistic $A + A$ collisions can be divided into three limiting groups: transparency (T), mixing (M), and reflection (R) models. The rapidity distributions resulting from the T, M, and R models are sketched in Fig. 2 taken from Ref. [18]. We note that there are models that assume the mixing of hadron production sources but the transparency of baryon flows, e.g., the three-fluid hydrodynamical model [19]. R models appear rather unrealistic and are included for completeness in our discussion.

III. NET BARYON NUMBER FLUCTUATIONS

We begin with a quantitative discussion by first considering the fluctuations of the net baryon number in different regions of the participant domain in collisions of two identical nuclei. These fluctuations are most closely related to the fluctuations of the number of participant nucleons because of baryon number conservation.

The HSD results for ω_B in Pb+Pb at 158A GeV are presented in Fig. 3. In each event we subtract the nucleon spectators when counting the number of baryons. The net baryon number in the full phase space, $B \equiv N_B - N_{\overline{B}}$, equals then the total number of participants $N_P = N_P^{\rm targ} + N_P^{\rm proj}$. At fixed $N_P^{\rm proj}$, the N_P number fluctuates because of fluctuations of $N_P^{\rm targ}$. These fluctuations correspond to an average value, $\langle N_P^{\rm targ}\rangle \simeq N_P^{\rm proj}$, and a scaled variance, $\omega_P^{\rm targ}$ (see Fig. 1). Thus, for the net baryon number fluctuations in the full phase space

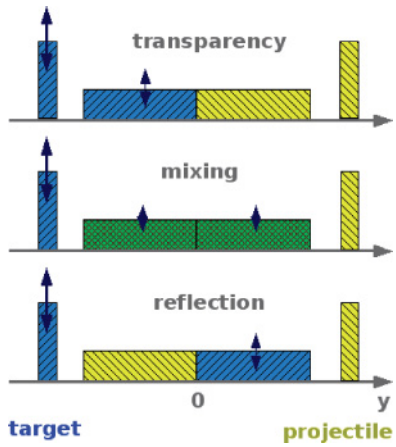

FIG. 2. (Color online) The sketch of the rapidity distributions of the baryon number or the particle production sources (horizontal rectangles) in nucleus-nucleus collisions resulting from the transparency, mixing, and reflection models. The spectator nucleons are indicated by the vertical rectangles. In the collisions with a fixed number of projectile spectators only matter related to the target shows significant fluctuations (vertical arrows). See Ref. [18] for more details.

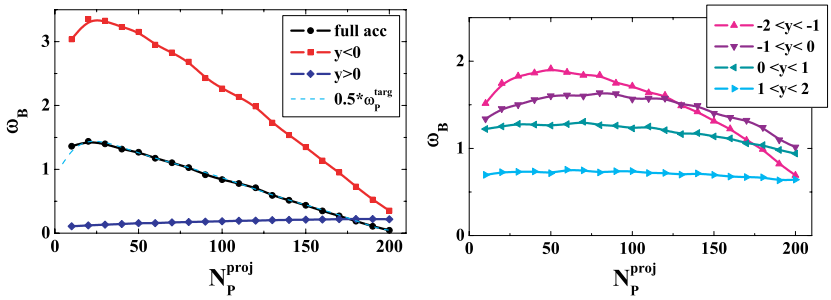

FIG. 3. (Color online) The HSD simulations for Pb+Pb collisions at 158A GeV for fixed values of $N_P^{\rm proj}$. (Left) The baryon number fluctuations in full acceptance, ω_B, in projectile hemisphere, ω_B^p (lower curve), and in target hemisphere, ω_B^t (upper curve). The dashed line, $0.5\omega_P^{\rm targ}$, demonstrates the validity of the relation (1). (Right) The scaled variances of the baryon number fluctuations in different rapidity intervals.

we find,

$$\omega_B = \frac{\mathrm{Var}(N_P)}{\langle N_P\rangle} \simeq \frac{\langle (N_P^{\rm targ})^2\rangle - \langle N_P^{\rm targ}\rangle^2}{2\langle N_P^{\rm targ}\rangle} = \frac{1}{2}\omega_P^{\rm targ}. \quad (1)$$

A factor $1/2$ on the right-hand side of Eq. (1) appears because only half of the total number of participants fluctuates.

Let us introduce ω_B^p and ω_B^t, where the superscripts p and t mark quantities measured in the projectile and target momentum hemispheres, respectively. Figure 3 demonstrates that $\omega_B^t > \omega_B^p$, both in the whole projectile-target hemispheres and in the symmetric rapidity intervals. On the other hand one observes that $\omega_B^p \approx \omega_B^t$ in most central collisions. This is because the fluctuations of the target participants become negligible in this case, i.e., $\omega_P^{\rm targ} \to 0$ (Fig. 1, right). As a consequence the fluctuations of any observable in the symmetric rapidity intervals become identical in most central collisions. Note also that transparency-mixing effects are different at different rapidities. From Fig. 1 (right) it follows that ω_B^p in the target rapidity interval $[-2,-1]$ is much larger than ω_B^t in the symmetric projectile rapidity interval [1,2]. This fact reveals the strong transparency effects. On the other hand, the behavior is different in symmetric rapidity intervals near the midrapidity. From Fig. 1 (right) one observes that ω_B^p in the target rapidity interval $[-1,0]$ is already much closer to ω_B^t in the symmetric projectile rapidity interval $[0,1]$. This gives a rough estimate of the width, $\Delta y \approx 1$, for the region in the rapidity space where projectile and target nucleons communicate with each others.

By assumption, the mixing of the projectile and target participants is absent in T and R models. Therefore, in T models, the net baryon number in the projectile hemisphere equals $N_p^{\rm proj}$ and does not fluctuate, i.e., $\omega_B^p(T) = 0$, whereas the net baryon number in the target hemisphere equals to $N_p^{\rm targ}$ and fluctuates with $\omega_B^t(T) = \omega_P^{\rm targ}$. These relations are reversed in R models. We introduce now a mixing of baryons between the projectile and target hemispheres. Let α be the probability for a (projectile) target participant to be detected in the (target) projectile hemisphere. We denote by n^t and n^p the number of baryons that end up in the target and projectile hemispheres, respectively, from the opposite hemisphere. Then the probabilities to detect B^t baryons in the target hemisphere and B^p baryons in the projectile hemisphere can be written as

$$P(B^t; N_P^{\rm proj}) = \sum_{N_P^{\rm targ}} W(N_P^{\rm targ}; N_P^{\rm proj}) \sum_{n^t=1}^{N_P^{\rm targ}} \sum_{n^p=1}^{N_P^{\rm proj}} \alpha^{n^p}(1-\alpha)^{N_P^{\rm targ}-n^p} \times \frac{N_P^{\rm targ}!}{n^p!(N_P^{\rm targ}-n^p)!}\alpha^{n^t}(1-\alpha)^{N_P^{\rm proj}-n^t} \times \frac{N_P^{\rm proj}!}{n^t!(N_P^{\rm proj}-n^t)!}\delta(B^t - N_P^{\rm targ} - n^t + n^p), \quad (2)$$

$$P(B^p; N_P^{\rm proj}) = \sum_{N_P^{\rm targ}} W(N_P^{\rm targ}; N_P^{\rm proj}) \sum_{n^t=1}^{N_P^{\rm targ}} \sum_{n^p=1}^{N_P^{\rm proj}} \alpha^{n^p}(1-\alpha)^{N_P^{\rm targ}-n^p} \times \frac{N_P^{\rm targ}!}{n^p!(N_P^{\rm targ}-n^p)!}\alpha^{n^t}(1-\alpha)^{N_P^{\rm proj}-n^t} \times \frac{N_P^{\rm proj}!}{n^t!(N_P^{\rm proj}-n^t)!}\delta(B^p - N_P^{\rm proj} - n^p + n^t), \quad (3)$$

where $W(N_P^{\rm targ}; N_P^{\rm proj})$ is the probability distribution of $N_P^{\rm targ}$ in a sample with fixed value of $N_P^{\rm proj}$. From Eqs. (2) and (3) with a straightforward calculation we find

$$\omega_B^t = (1-\alpha)^2\omega_P^{\rm targ} + 2\alpha(1-\alpha), \qquad \omega_B^p = \alpha^2\omega_P^{\rm targ} + 2\alpha(1-\alpha). \quad (4)$$

A (complete) mixing of the projectile and target participants is assumed in M models. Thus each participant nucleon with equal probability, $\alpha = 1/2$, can be found either in the target or in the projectile hemispheres. In M models the fluctuations in both projectile and target hemispheres are identical. The limiting cases, $\alpha = 0$ and $\alpha = 1$, of Eq. (4) correspond to T and R models, respectively. In summary, the scaled variances of the net baryon number fluctuations in the projectile, ω_B^p, and target, ω_B^t, hemispheres are

$$\omega_B^p(T) = 0, \quad \omega_B^t(T) = \omega_P^{\rm targ}, \quad (5)$$

$$\omega_B^p(M) = \omega_B^t(M) = \tfrac{1}{2} + \tfrac{1}{4}\omega_P^{\rm targ}, \quad (6)$$

$$\omega_B^p(R) = \omega_P^{\rm targ}, \quad \omega_B^t(R) = 0, \quad (7)$$

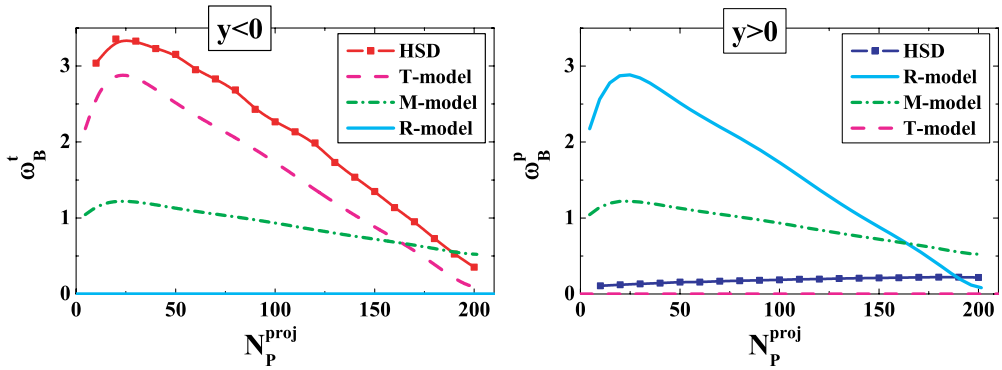

FIG. 4. (Color online) The ω_B^t (left) and ω_B^p (right) of the HSD simulations in comparison to T, M, and R models (5)–(7), with $\omega_P^{\rm targ}$ taken from Fig. 1.

in the T (5), M (6) and R (7) models of the baryon number flow. The different models lead to significantly different predictions for ω_B^p and ω_B^t.

In Fig. 4 we show the predictions of T, M, and R models (5)–(7) with $\omega_P^{\rm targ}$ from Fig. 1 for Pb+Pb collisions at 158A GeV. From Fig. 4 one concludes that the HSD results are close to the T-model estimates for baryon flow. However, the deviations from the results (5) are clearly seen: $\omega_B^p > 0$ and $\omega_B^t > \omega_P^{\rm targ}$. One cannot fit the HSD values of ω_B^t and ω_B^p by Eq. (4). To make $\omega_B^p > 0$ one needs $\alpha > 0$, but this induces $\omega_B^t < \omega_P^{\rm targ}$, i.e., a mixing of baryons between the projectile and target hemispheres creates a non-zero baryon number fluctuation in the projectile hemisphere on the expense of fluctuations in the target hemisphere. Indeed, it follows from Eq. (4) that ω_B^p increases with α for all α, if $\omega_P^{\rm targ} > 1$, and for $\alpha < (2 - \omega_P^{\rm targ})^{-1}$, if $\omega_P^{\rm targ} < 1$. On the other hand, ω_B^t increases with α if $\alpha < (1 - \omega_P^{\rm targ})(2 - \omega_P^{\rm targ})^{-1}$. This shows that an increase of ω_B^t with α is only possible for $\omega_P^{\rm targ} < 1$. Thus for $\omega_P^{\rm targ} > 1$ one finds an increase of ω_B^p with α and a decrease of ω_B^t with α for all physical values of α from 0 to 1. Therefore, we conclude that the HSD values of ω_B^t (i.e., the fact that $\omega_B^t > \omega_P^{\rm targ}$) cannot be explained by Eq. (4) with $\alpha > 0$.

The numbers of target and projectile participants are defined as $N_P^{\rm targ} \equiv A - N_S^{\rm targ}$ and $N_P^{\rm proj} \equiv A - N_S^{\rm proj}$. The actual event-by-event numbers of baryons in the target and projectile hemispheres, N_B^t and N_B^p, may differ from $N_P^{\rm targ}$ and $N_P^{\rm proj}$. This is because a transfer of baryons between the projectile and target hemispheres arises from the production of baryon-antibaryon pairs. The partners of each newly created $b\bar{b}$-pair can be detected with non-zero probability in different hemispheres. We introduce $b^t \equiv N_B^t - N_P^{\rm targ}$ and the number of antibaryons in the target hemisphere, $\bar{b}^t$. Similarly, $b^p \equiv N_B^p - N_P^{\rm proj}$, while $\bar{b}^p$ is the number of antibaryons in the projectile hemisphere. One finds

$$\omega_B^t \equiv \frac{\mathrm{Var}\left(N_P^{\rm targ} + b^t - \bar{b}^t\right)}{\langle B^t\rangle} = \omega_P^{\rm targ} + \frac{1}{N_P^{\rm proj}}\left[\mathrm{Var}(b^t) + \mathrm{Var}(\bar{b}^t) + 2\Delta\left(N_P^{\rm targ}, b^t\right) - 2\Delta\left(N_P^{\rm targ}, \bar{b}^t\right) - 2\Delta(b^t, \bar{b}^t)\right], \quad (8)$$

$$\omega_B^p \equiv \frac{\mathrm{Var}\left(N_P^{\rm proj} + b^p - \bar{b}^p\right)}{\langle B^p\rangle} = \frac{1}{N_P^{\rm proj}}[\mathrm{Var}(b^p) + \mathrm{Var}(\bar{b}^p) - 2\Delta(b^p, \bar{b}^p)], \quad (9)$$

where

$$\Delta(N_1, N_2) \equiv \langle N_1 \cdot N_2\rangle - \langle N_1\rangle \cdot \langle N_2\rangle. \quad (10)$$

As $N_P^{\rm proj} = \mathrm{const}$ in the sample, it follows that $\omega_P^{\rm proj} = 0$, $\Delta(N_P^{\rm proj}, b^p) = 0$, $\Delta(N_P^{\rm proj}, \bar{b}^p) = 0$; these terms are absent in the r.h.s. of Eq. (9). Different terms of Eqs. (8) and (9) found

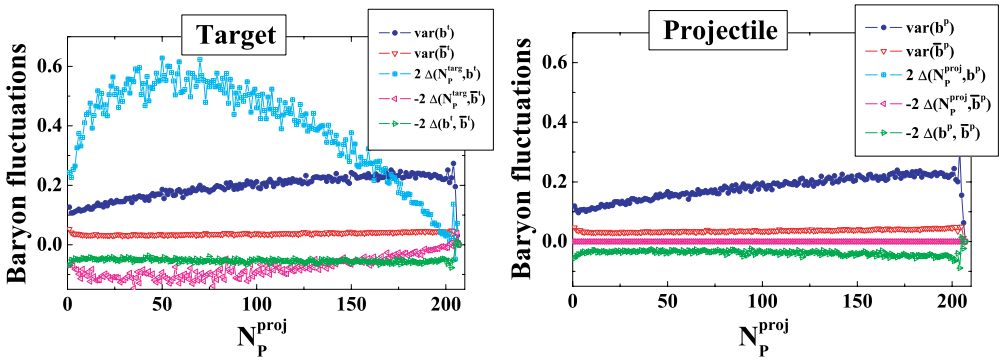

FIG. 5. (Color online) Different terms of Eq. (8), left, and Eq. (9), right, are presented as a function of $N_P^{\rm proj}$.

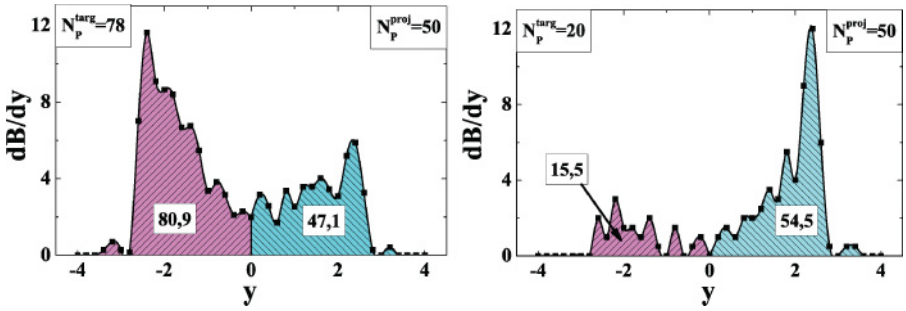

FIG. 6. (Color online) The HSD results for Pb+Pb collisions at 158A GeV for the rapidity distributions of baryon numbers in nonsymmetric samples with $N_P^{\rm proj} = 50$, $N_P^{\rm targ} = 78$ (left) and $N_P^{\rm proj} = 50$, $N_P^{\rm targ} = 20$ (right).

from the HSD simulations are presented in Fig 5. One observes that the terms of Eqs. (8) and (9) expressing the fluctuations of antibaryons, $\mathrm{Var}(\overline{b}^p)/N_P^{\rm proj}$, and the correlation terms, $2\Delta(N_P^{\rm targ}, \overline{b}^t)/N_P^{\rm proj}$ and $-2\Delta(b^t, \overline{b}^t)/N_P^{\rm proj}$, with antibaryons included, are small. Therefore, one finds, $\omega_B^p \cong \mathrm{Var}(b^p)/N_P^{\rm proj}$. In the target hemisphere, the $\omega_P^{\rm targ}$ gives the main contribution to ω_B^t in Eq. (8). The term $\mathrm{Var}(b^t)/N_P^{\rm proj}$ also contributes to ω_B^t, similarly to that, $\mathrm{Var}(b^p)/N_P^{\rm proj}$, in the projectile hemisphere. However, the main additional term to ω_B^t is $2\Delta(N_P^{\rm targ}, b^t)/N_P^{\rm proj}$, which is due to (positive) correlations between $N_P^{\rm targ}$ and b^t. This implies that in events with large $N_P^{\rm targ}$ (i.e., $N_P^{\rm targ} > \langle N_P^{\rm targ}\rangle \cong N_P^{\rm proj}$) some additional baryons move from the projectile to the target hemisphere, and when $N_P^{\rm targ}$ is small (i.e., $N_P^{\rm targ} < \langle N_P^{\rm targ}\rangle \cong N_P^{\rm proj}$) the baryons move in the reverse direction from the target to the projectile hemisphere as shown in Fig. 6.

This HSD result looks rather unexpected. We note that Eq. (4) predicts for ω_B^t the opposite behavior: because of a simple mixing of baryons between the target and projectile hemispheres the initially large fluctuations, $\omega_P^{\rm targ}$, are transformed into smaller ones, ω_B^t. It seems that the origin of this effect is the following: For $N_P^{\rm targ} > N_P^{\rm proj}$ each projectile nucleon interacts, in average, more often than the target nucleon. The projectile participant loses then a larger part of its energy, and in the rapidity space its position becomes closer to $y_{\rm c.m.} = 0$ than the position of target participants. This gives to projectile participants more chances to move due to further rescatterings from projectile to target hemisphere, in comparison with target participants to move in the opposite direction. For $N_P^{\rm targ} < N_P^{\rm proj}$ there is a reverse situation. This fact was not taken into account in Eqs. (2) and (3) where it has been assumed that the mixing probability α is the same for projectile and target participants and independent of $N_P^{\rm targ}$.

IV. NET ELECTRIC CHARGE FLUCTUATIONS

The T, M, and R models give very different predictions for ω_B^p and ω_B^t for the samples of events with fixed values of $N_P^{\rm targ}$. Additional interesting correlations between the B^t and B^p numbers, such as those seen in the HSD simulations, can be expected. Unfortunately, they may be difficult to test experimentally as an identification of protons and a measurement of neutrons in a large acceptance in a single event is difficult. Measurements of the charged particle multiplicity in a large acceptance can be performed with the existing detectors. In this section we consider the HSD results for the net electric charge, Q, fluctuations. As $Q \cong 0.4B$ in the initial heavy nuclei one can naively expect that Q fluctuations are quite similar to B fluctuations. We stress, however, a principal difference between Q and B in relativistic $A + A$ collisions. Figure 7 demonstrates the rapidity distributions of the net baryon number, $B = N_B - N_{\overline{B}}$ (left), and *total* number of baryons, $N_B + N_{\overline{B}}$ (right), for different centralities in Pb+Pb collisions at 158A GeV. One observes that both quantities are very close to each other; the y dependence and absolute values are very close for B and $N_B - N_{\overline{B}}$ distributions. This is, of course, because the number of antibaryons is rather small, $N_{\overline{B}} \ll N_B$.

Figure 8 shows the same as Fig. 7 but for the electric charge $Q = N_+ - N_-$ (left) and the *total* number of charged particles, $N_{\rm ch} \equiv N_+ + N_-$ (right). The y dependence of dQ/dy and

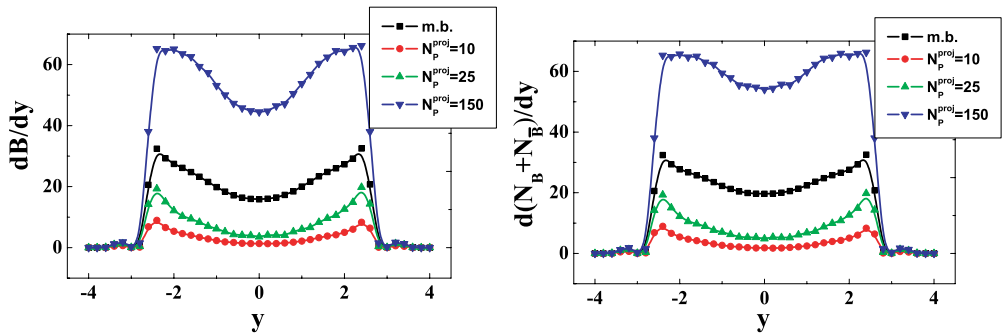

FIG. 7. (Color online) The HSD rapidity distributions in Pb+Pb collisions at 158A GeV for the net baryon number, $B = N_B - N_{\overline{B}}$ (left), and total number of baryons, $N_B + N_{\overline{B}}$ (right), at different $N_P^{\rm proj}$ and in the minimum bias (m.b.) sample.

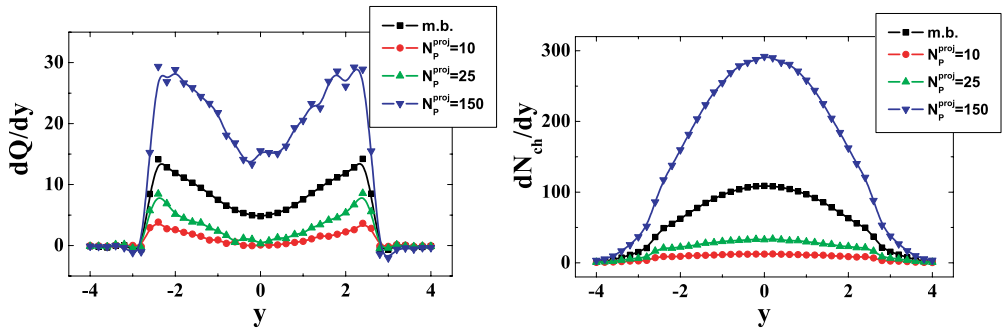

FIG. 8. (Color online) The same as in Fig. 7 but for the electric charge $Q = N_+ - N_-$ (left), and total number of charged particles, $N_{\rm ch} \equiv N_+ + N_-$ (right).

$dN_{\rm ch}/dy$ is quite different. Besides, the absolute values of $N_{\rm ch}$ are about 10 times larger than those of Q. This implies that $Q \ll N_+ \approx N_-$.

In the previous section we use the scaled variance ω_B to quantify the measure of the net baryon fluctuations. It appears to be a useful variable as ω_B is straightforwardly connected to $\omega_P^{\rm targ}$ and due to the relatively small number of antibaryons. Figure 8 shows that ω_Q is a bad measure of the electric charge fluctuations in high energy $A + A$ collisions. One observes that $\omega_Q \equiv {\rm Var}(Q)/\langle Q\rangle$ is much larger than 1 simply because of the small value of $\langle Q\rangle$ in a comparison with N_+ and N_-. If the $A + A$ collision energy increases, it follows $\langle Q\rangle \to 0$, and thus $\omega_Q \to \infty$. The same will happen with ω_B, too, at much larger energies. A useful measure of the net electric charge fluctuations is the quantity (see, e.g., [10])

$$X_Q \equiv \frac{{\rm Var}(Q)}{\langle N_{\rm ch}\rangle}. \tag{11}$$

A value of X_Q can be easily calculated for the Boltzmann ideal gas in the grand canonical ensemble. In this case the number of negative and positive particles fluctuates according to the Poisson distribution (i.e., $\omega_- = \omega_+ = 1$), and the correlation between N_+ and N_- is absent (i.e., $\langle N_+N_-\rangle = \langle N_+\rangle\langle N_-\rangle$), so that $X_Q = 1$. On the other hand, the canonical ensemble formulation (i.e., when $Q = {\rm const}$ fixed exactly for all microscopic states of the system) leads to $X_Q = 0$.

Figure 9 shows the results of the HSD simulations for the full acceptance, for the projectile and target hemispheres (left), and also for symmetric rapidity intervals in the c.m.s. (right).

The Q fluctuation in the full acceptance is due to $N_P^{\rm targ}$ fluctuations. As $Q \cong 0.4B$ in colliding (heavy) nuclei, one may expect ${\rm Var}(Q) \cong 0.16\,{\rm Var}(B)$. In addition, $\langle N_{\rm ch}\rangle \cong 4\langle N_P\rangle$ at $158A$ GeV, so that one estimates $X_Q \cong 0.04\,\omega_B$ for the fluctuations in the full phase space. The actual values of X_Q presented in Fig. 9 (left) are about three times larger. This is because of Q fluctuations due to different event-by-event values of proton and neutron participants even in a sample with fixed values of $N_P^{\rm proj}$ and $N_P^{\rm targ}$.

From Fig. 9 (right) one sees only a tiny difference between the X_Q values in the symmetric rapidity intervals in the projectile and target hemispheres and slightly stronger effects for the whole projectile and target hemispheres (Fig. 9, right). In fact, the fluctuations of N_+ and N_- are very different in the projectile and target hemispheres, and the scaled variances ω_+^t and ω_-^t have a very strong $N_P^{\rm proj}$ dependence. This is shown in Fig. 10 obtained in our previous study [17].

The X_Q can be presented in two equivalent forms

$$\begin{aligned} X_Q &= \omega_+\frac{\langle N_+\rangle}{\langle N_{\rm ch}\rangle} + \omega_-\frac{\langle N_-\rangle}{\langle N_{\rm ch}\rangle} - 2\frac{\Delta(N_+, N_-)}{\langle N_{\rm ch}\rangle} \\ &= 2\omega_+\frac{\langle N_+\rangle}{\langle N_{\rm ch}\rangle} + 2\omega_-\frac{\langle N_-\rangle}{\langle N_{\rm ch}\rangle} - \omega_{\rm ch}. \end{aligned} \tag{12}$$

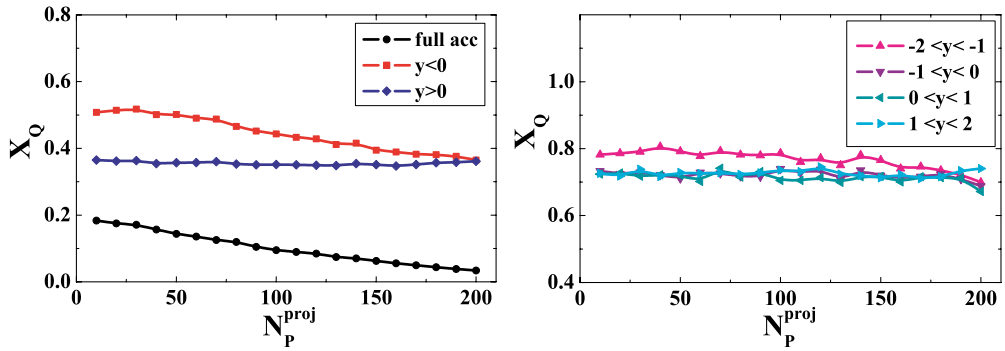

FIG. 9. (Color online) (Left) The HSD simulations in Pb+Pb collisions at $158A$ GeV for X_Q at different values of $N_P^{\rm proj}$ in the full acceptance (lower curve), for the projectile hemisphere (middle curve), and for the target hemisphere (upper curve). (Right) The same, but for symmetric rapidity intervals in the c.m.s.

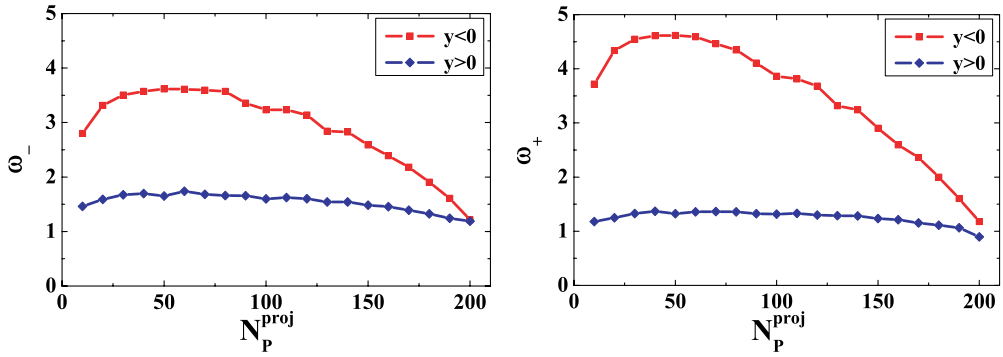

FIG. 10. (Color online) The HSD results for the scaled variances of negatively (left) and positively (right) charged hadrons in Pb+Pb collisions at 158A GeV for the projectile (lower curves) and target (upper curves) hemispheres.

Equation (12) is valid for any region of the phase space: full phase space, projectile or target hemisphere, etc. As seen from Fig. 10, both ω_+^t and ω_-^t are large and strongly $N_P^{\rm proj}$-dependent. This is not seen in X_Q^t because of strong correlations between N_+^t and N_-^t, i.e., the term $2\Delta(N_+, N_-)/\langle N_{\rm ch}\rangle$ compensates the ω_+ and ω_- terms in Eq. (12). This is also seen from Fig. 11. A cancellation of strong $N_P^{\rm proj}$ dependence in the target hemisphere takes place between the sum of ω_+^t and ω_-^t terms of Eq. (12), and the $\omega_{\rm ch}^t$ term.

Figure 12 shows a comparison of the HSD results for X_Q with NA49 data in Pb+Pb collisions at 158A GeV for the forward rapidity interval $1.1 < y < 2.6$ inside the projectile hemisphere with an additional p_T filter imposed. As an illustration, the HSD results in the symmetric backward rapidity interval $-2.6 < y < -1.1$ (target hemisphere) are also included. One observes no difference between the X_Q results for the NA49 acceptance in the projectile and target hemispheres. The HSD values for ω_+, ω_-, and $\omega_{\rm ch}$ are rather different in the projectile and target hemispheres for the NA49 acceptance (see Figs. 10 and 11). This is not seen in Fig. 12 for X_Q. As explained above a cancellation between the ω_+, ω_-, and $\omega_{\rm ch}$ terms takes place in Eq. (12). In fact, NA49 did not perform the X_Q measurements. The X_Q data (solid dots) presented in Fig. 12 are obtained from Eq. (12) using the NA49 data for ω_+, ω_-, and $\omega_{\rm ch}$ as well as $\langle N_+\rangle$, $\langle N_-\rangle$, and $\langle N_{\rm ch}\rangle$ [20]. Such a procedure leads, however, to very large errors for X_Q (which are not indicated in Fig. 12), which excludes any conclusion about the (dis)agreement of HSD results with NA49 data.

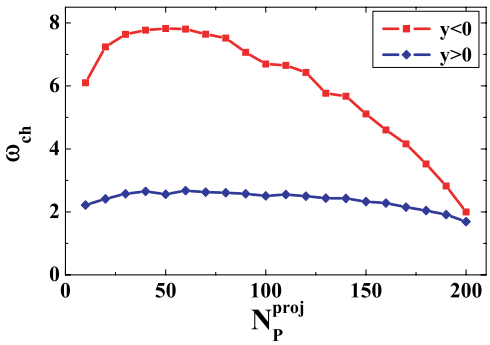

FIG. 11. (Color online) The HSD results for the scaled variances of all charged hadrons, $\omega_{\rm ch}$, in Pb+Pb collisions at 158A GeV for the projectile (lower curve) and target (upper curve) hemispheres.

V. FLUCTUATIONS IN MOST CENTRAL COLLISIONS

In this section we consider the baryon number and electric charge fluctuations in the symmetric rapidity interval $[-y, y]$ in the c.m.s. for the most central Pb+Pb events. We chose the sample of most central events by restricting the impact parameter to $b < 2$ fm. It gives about 2% of the most central Pb+Pb collisions from the whole minimum bias sample. Figure 13 shows the HSD results for electric charge fluctuations in 2% of the most central Pb+Pb collisions for the symmetric rapidity interval $\Delta Y = [-y, y]$ in the c.m.s. as the function of $\Delta y = \Delta Y/2$. For $\Delta Y \to 0$, one finds $X_Q \to 1$. This can be understood as follows: For $\Delta Y \to 0$ the fluctuations of negatively, positively, and all charged particles behave as for the Poisson distribution: $\omega_+ \cong \omega_- \cong \omega_{\rm ch} \cong 1$. Then from Eq. (12) it follows that $X_Q \cong 1$, too. From Fig. 13 (right) one observes that ω_+, ω_-, and $\omega_{\rm ch}$ all increase with the increasing interval ΔY. However, X_Q decreases with ΔY and—because

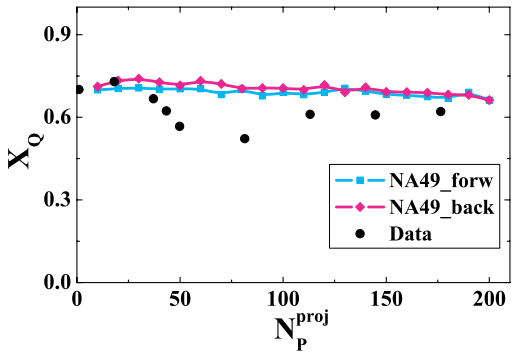

FIG. 12. (Color online) The HSD results for X_Q for Pb+Pb collisions at 158A GeV for the forward rapidity interval $1.1 < y < 2.6$ inside the projectile hemisphere. The solid dots are the estimates obtained from Eq. (12) using the NA49 experimental data [20] (the error bars are not indicated here). For illustration, the HSD results in the symmetric backward rapidity interval $-2.6 < y < -1.1$ (target hemisphere) are also presented.

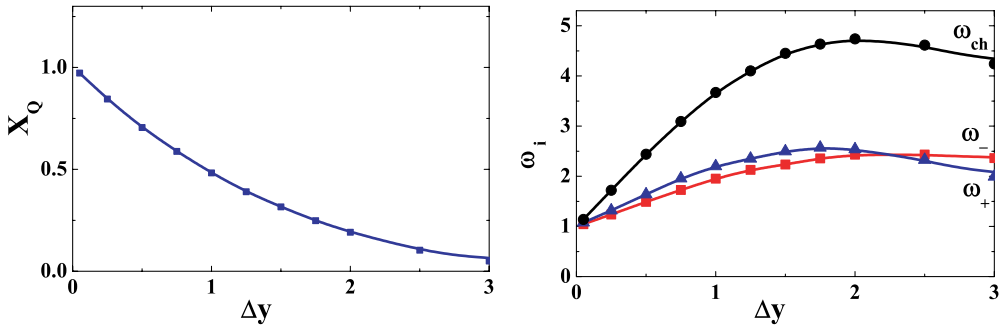

FIG. 13. (Color online) The HSD results for electric charge fluctuations in 2% of the most central Pb+Pb collisions at 158A GeV in the symmetric rapidity interval $\Delta Y = [-y, y]$ as a function of $\Delta y = \Delta Y/2$ in the c.m.s. The left panel shows the behavior of X_Q, and the right one demonstrates separately ω_+, ω_-, and $\omega_{\rm ch}$.

of global Q conservation—it goes approximately to zero when all final particles are accepted.

In Fig. 14 (left) the HSD results for the scaled variances are presented in full acceptance as functions of $N_P^{\rm proj}$. Figure 14 (right) demonstrates the probability distribution of events with $b < 2$ fm over $N_P^{\rm proj}$. One observes that even in the 2% centrality sample the values of $N_P^{\rm proj}$ are noticeably smaller than the maximum value, $A = 208$. As seen from Fig. 14 (left) the HSD values of ω_+, ω_-, and $\omega_{\rm ch}$ become then essentially larger than 1 in agreement with those presented in Fig. 13.

Figure 15 shows the net baryon number fluctuations in the symmetric rapidity interval $[-y, y]$ in the c.m.s. as the function of ΔY. As a measure of the net baryon number fluctuations we have used the quantity,

$$X_B \equiv \frac{\mathrm{Var}(B)}{\langle N_B + N_{\overline{B}}\rangle}. \tag{13}$$

As for the electric charge, one finds that $X_B \to 1$ at $\Delta Y \to 0$ (this is because all ω_{N_B}, $\omega_{N_{\overline{B}}}$, and $\omega_{N_B+N_{\overline{B}}}$ go to 1 in this limit (see Fig. 15, left), and $X_B \to 0$ at upper limit of ΔY because of global baryon number conservation.

Writing the variance $\mathrm{Var}(B)$ in the form,

$$\mathrm{Var}(B) = 2\mathrm{Var}(N_B) + 2\mathrm{Var}(N_{\overline{B}}) - \mathrm{Var}(N_B + N_{\overline{B}}), \tag{14}$$

we find

$$X_B = 2\omega_{N_B}\frac{\langle N_B\rangle}{\langle N_B + N_{\overline{B}}\rangle} + 2\omega_{N_{\overline{B}}}\frac{\langle N_{\overline{B}}\rangle}{\langle N_B + N_{\overline{B}}\rangle} - \omega_{N_B+N_{\overline{B}}}. \tag{15}$$

The behavior of the different terms in Eq. (15) is the following: As seen from Fig. 15, right, $\omega_{N_{\overline{B}}} \cong 1$ for all values of ΔY. This is because $N_{\overline{B}} \ll N_B$, and baryon number conservation does not affect the fluctuations of antibaryons. Due to the small number of antibaryons in comparison to baryons, one also observes $\omega_B \cong \omega_{N_B} \cong \omega_{N_B+N_{\overline{B}}}$.

VI. ELECTRIC CHARGE FLUCTUATIONS IN CENTRAL Pb + Pb COLLISIONS AT 20, 30, 40, 80, AND 160A GeV

In this section we present the HSD results for the event-by-event electric charge fluctuations as measured by the NA49 Collaboration in central Pb+Pb collisions at 20A, 30A, 40A, 80A, and 160A GeV [22]. The interest in this observable (as a signal of deconfinement) is related to the predicted (in Refs. [23,24]) suppression of event-by-event fluctuations of the electric charge in a quark-gluon plasma (QGP) relative to a hadron gas. However, these predictions were based on the assumption that the initial electric charge fluctuations survive the hadronization phase.

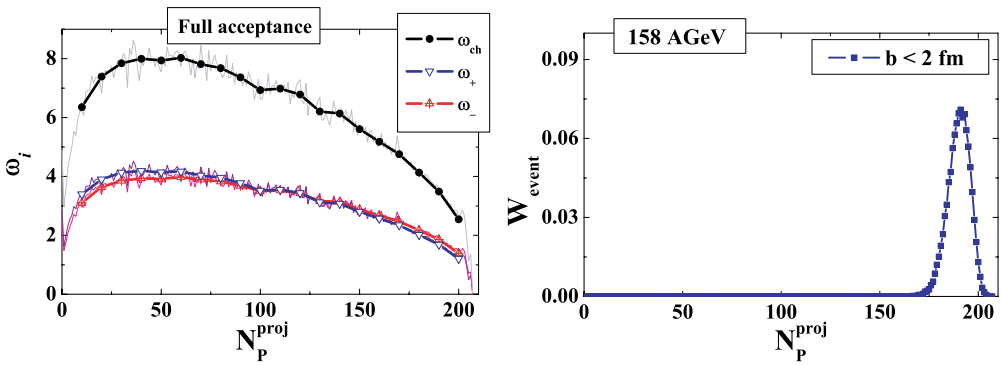

FIG. 14. (Color online) The HSD results in Pb+Pb collisions at 158A GeV. (Left) The scaled variances ω_+, ω_-, and $\omega_{\rm ch}$ in the full acceptance. (Right) The distributions of events over $N_P^{\rm proj}$ in the most central collisions with $b < 2$ fm.

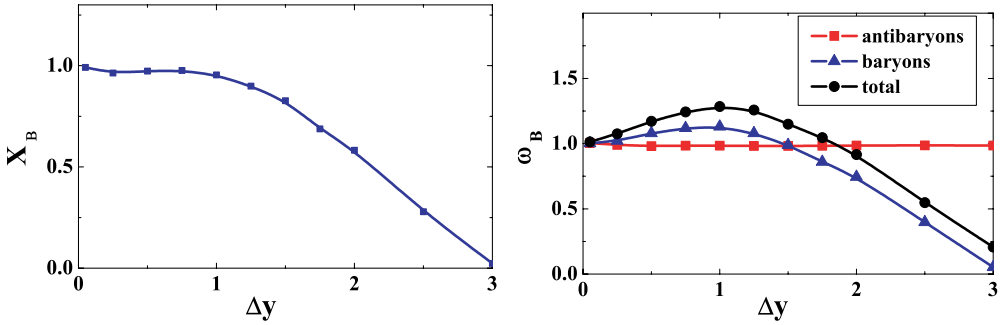

FIG. 15. (Color online) The HSD results for net baryon number fluctuations in 2% most central Pb+Pb collisions at 158 AGeV in the symmetric rapidity interval $\Delta Y = [-y, y]$ as a function of $\Delta y = \Delta Y/2$ in the c.m.s. The *left* panel shows the behavior of X_B, and a *right* panel presents separately ω_{N_B}, $\omega_{N_{\overline{B}}}$, and $\omega_{N_B+N_{\overline{B}}}$.

The first experimental measurement of charge fluctuations in central heavy-ion collisions by PHENIX [25] and STAR [26] at the Relativistic Heavy Ion Collider (RHIC) and by the NA49 [22] at SPS showed a quite moderate suppression of the electric charge fluctuations. This observation has been attributed to the fact that the initial fluctuations are distorted by the hadronization. In particular, the observed fluctuations might be related to the final resonance decays.

In this respect it is important to compare the experimental data with the results of microscopic transport models such as HSD where the resonance decays are included by default. To quantify the event-by-event electric charge fluctuations we have calculated the quantity Φ defined as [22,27]

$$\Phi_q = \sqrt{\frac{\langle Z^2\rangle}{\langle N\rangle}} - \sqrt{\overline{z^2}}, \tag{16}$$

where

$$z = q - \overline{q}, \quad Z = \sum_{i=1}^{N}(q_i - \overline{q}). \tag{17}$$

Here q denotes a single particle variable, i.e., electric charge q; N is the number of particles of the event within the acceptance; and the overbars and angle brackets denote averaging over a single particle inclusive distribution and over events, respectively. By construction, Φ of the system, which is an independent sum of identical sources of particles, is equal to the Φ for a single source [27,28].

To remove the sensitivity of the final signal to the trivial global charge conservation (GCC) the measure $\Delta\Phi_q$ is defined as the difference

$$\Delta\Phi_q = \Phi_q - \Phi_{q,\mathrm{GCC}}. \tag{18}$$

Here the value of Φ_q is given by [29,30]

$$\Phi_{q,\mathrm{GCC}} = \sqrt{1-P} - 1, \tag{19}$$

where

$$P = \frac{\langle N_{\mathrm{ch}}\rangle}{\langle N_{\mathrm{ch}}\rangle_{\mathrm{tot}}} \tag{20}$$

with $\langle N_{\mathrm{ch}}\rangle$ and $\langle N_{\mathrm{ch}}\rangle_{\mathrm{tot}}$ being the mean charged multiplicity in the detector acceptance and in the full phase space (excluding spectator nucleons), respectively.

By construction, the value of $\Delta\Phi_q$ is zero if the particles are correlated by global charge conservation only. It is negative in the case of an additional correlation between positively and

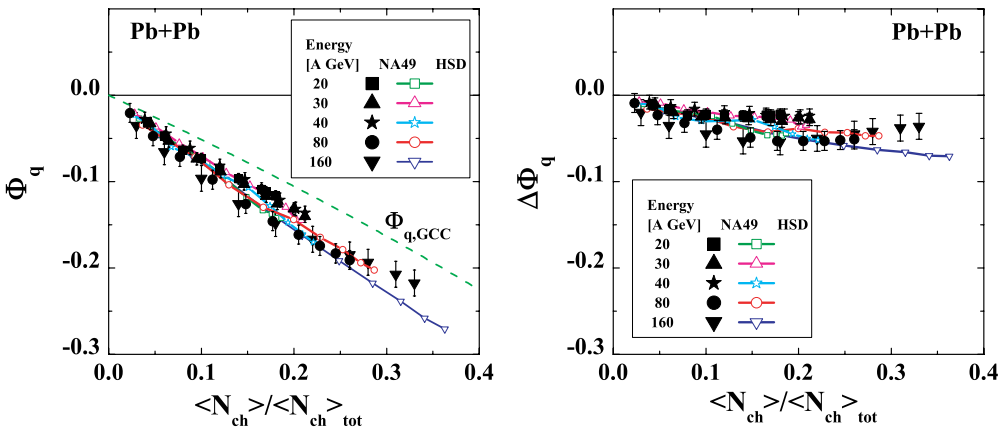

FIG. 16. (Color online) The dependence of the Φ_q (l.h.s.) and $\Delta\Phi_q$ (r.h.s.) on the fraction of accepted particles for central Pb+Pb collisions at 20A–158A GeV. The NA49 data [22] are shown as solid symbols, whereas the open symbols (connected by lines) represent the HSD results. The dashed line shows the dependence expected for the case if the only source of particle correlations is the global charge conservation $\Phi_{q,\mathrm{GCC}}$, Eq. (19).

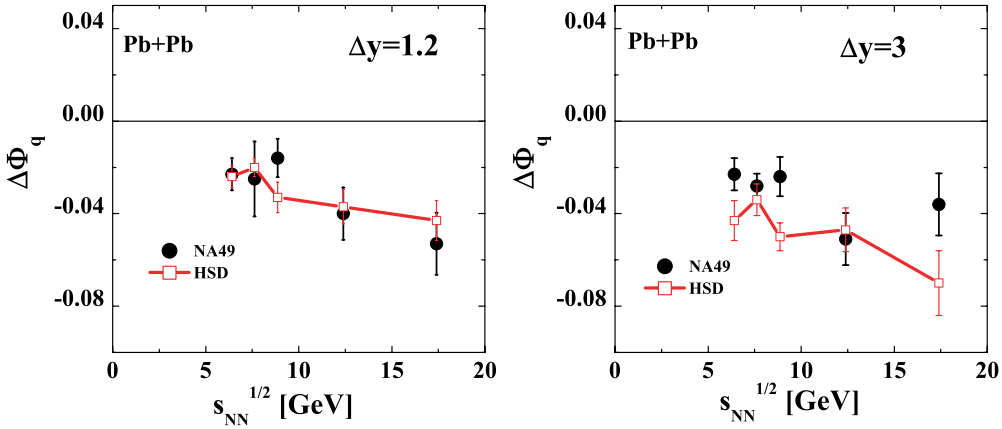

FIG. 17. (Color online) The energy dependence of $\Delta\Phi_q$ measured in central Pb+Pb collisions for a narrow rapidity interval $\Delta y = 1.2$ (l.h.s.) and a broad rapidity interval $\Delta y = 3$ (r.h.s.). The NA49 data [22] are shown as solid symbols, whereas the the open symbols (connected by lines) reflect the HSD results.

negatively charged particles, and it is positive if the positive and negative particles are anti-correlated [30].

Figure 16 shows the HSD results for the dependence of Φ_q (l.h.s.) and $\Delta\Phi_q$ (r.h.s.) on the fraction of accepted particles $\langle N_{\rm ch}\rangle$ and $\langle N_{\rm ch}\rangle_{\rm tot}$ (calculated for ten different rapidity intervals increasing in size from $\Delta y = 0.3$ to $\Delta y = 3$ in equal steps) for central Pb+Pb collisions at $20A, 30A, 40A, 80A$, and $158A$ GeV. The NA49 data [22] are shown as full symbols, whereas the open symbols (connected by lines) reflect the HSD results. The dashed line shows the dependence expected for the case if the only source of particle correlations is the global charge conservation $\Phi_{q,\rm GCC}$ [Eq. (19)].

The data as well as the HSD results for Φ_q (Fig. 16, l.h.s.) are in a good agreement and show a monotonic decrease with increasing fraction of accepted particles. After substraction of the contribution by global charge conservation (the dashed line in Fig. 16), the values of $\Delta\Phi_q$ vary between 0 and -0.05, which are significantly larger than the values expected for QGP fluctuations ($-0.5 < \Delta\Phi_q < -0.15$ [30]).

Figure 17 presents the energy dependences of $\Delta\Phi_q$ for two selected rapidity intervals—the intermediate rapidity interval $\Delta y = 1.2$ (l.h.s.) and the largest rapidity interval $\Delta y = 3$ (r.h.s.). Both the data and the HSD results show a slight decrease of $\Delta\Phi_q$ with increasing energy.

The fact that the HSD model, which includes no explicit phase transition, describes the experimental data can be considered an independent proof that the event-by-event charge fluctuations are driven by the hadronization phase and dominantly by the resonance decays (which are naturally included in HSD) and are no longer sensitive to the initial phase fluctuations from a QGP.

VII. SUMMARY AND CONCLUSIONS

The goal of this study was to investigate the sensitivity of event-by-event fluctuations of baryon number and electric charge to the early stage dynamics of hot and dence nuclear matter created in heavy-ion collisions at SPS energies and the influence of the further hadronization and rescattering phase. For that purpose we explored the microscopic HSD transport model which allowed us to also investigate (on event-by-event basis) the influence of the experimental acceptance and the setup on the final observables.

It has been found that the fluctuations in the number of target participants strongly influences the baryon number and charged multiplicity fluctuations. The consequences of this fact depend crucially on the dynamics of the initial flows of the conserved charges and inelastic energy.

For a better quantitative understanding of the microscopic transport model (HSD) results we considered three limiting groups of models for nucleus-nucleus collisions: transparency, mixing, and reflection. These "pedagogical" considerations indicate that the HSD model (as well as UrQMD, cf. Ref. [17]) shows only a small mixing on initial baryon flow and is closer to the T model. This supports the findings from Ref. [2] about the influence of the partonic degrees of freedom on the initial phase dynamics which might increase the mixing by additional strong parton-parton interactions. Thus, the measurement of the net baryon number fluctuations helps to quantify the mixing of initial baryon flow.

The first microscopic event-by-event calculations of the charge fluctuations $\Delta\Phi_q$ within the HSD model show a good agreement with the NA49 data at SPS energies. Thus, this observable is dominated by the final stage dynamics, i.e., the hadronization phase and the resonance decays, and is rather insensitive to the initial QGP dynamics.

ACKNOWLEDGMENTS

We thank W. Cassing, M. Gaździcki, B. Lungwitz, I. N. Mishustin, St. Mrówczyński, M. Rybczyński, and L. M. Satarov for numerous discussions. The work was supported in part by the U.S. Civilian Research and Development Foundation (CRDF) Cooperative Grants Program, Project Agreement UKP1-2613-KV-04.

[1] W. Ehehalt and W. Cassing, Nucl. Phys. **A602**, 449 (1996); W. Cassing and E. L. Bratkovskaya, Phys. Rep. **308**, 65 (1999); W. Cassing, E. L. Bratkovskaya, and A. Sibirtsev, Nucl. Phys. **A691**, 753 (2001).

[2] H. Weber, E. L. Bratkovskaya, W. Cassing, and H. Stöcker, Phys. Rev. C **67**, 014904 (2003); E. L. Bratkovskaya, M. Bleicher, M. Reiter, S. Soff, H. Stöcker, M. van Leeuwen, S. A. Bass, and W. Cassing, *ibid.* **69**, 054907 (2004); E. L. Bratkovskaya, M. Bleicher, W. Cassing, M. Reiter, S. Soff, and H. Stöcker, Prog. Part. Nucl. Phys. **53**, 225 (2004); E. L. Bratkovskaya, W. Cassing, and H. Stöcker, Phys. Rev. C **67**, 054905 (2003).

[3] M. Gaździcki and St. Mrówczyński, Z. Phys. C **26**, 127 (1992).

[4] L. Stodolsky, Phys. Rev. Lett. **75**, 1044 (1995); E. V. Shuryak, Phys. Lett. **B423**, 9 (1998); St. Mrówczyński, *ibid.* **B430**, 9 (1998).

[5] G. Baym and H. Heiselberg, Phys. Lett. **B469**, 7 (1999).

[6] I. N. Mishustin, Phys. Rev. Lett. **82**, 4779 (1999); Nucl. Phys. **A681**, 56c (2001); H. Heiselberg and A. D. Jackson, Phys. Rev. C **63**, 064904 (2001).

[7] M. A. Stephanov, K. Rajagopal, and E. V. Shuryak, Phys. Rev. Lett. **81**, 4816 (1998); Phys. Rev. D **60**, 114028 (1999); M. A. Stephanov, Acta Phys. Pol. B **35**, 2939 (2004).

[8] S. Jeon and V. Koch, Phys. Rev. Lett. **83**, 5435 (1999); **85**, 2076 (2000).

[9] H. Heiselberg, Phys. Rep. **351**, 161 (2001).

[10] S. Jeon and V. Koch, *Published in Quark-Gluon Plasma 3*, edited by R. C. Hwa and X.-N. Wang (World Scientific, Singapore), Chap. 1, pp. 430–490 .

[11] M. Bleicher *et al*., Nucl. Phys. **A638**, 391 (1998); Phys. Lett. **B435**, 9 (1998); Phys. Rev. C **62**, 061902 (2000); **62**, 041901 (2000); S. Jeon, L. Shi, and M. Bleicher, Phys. Rev. C **73**, 014905 (2006); S. Haussler, H. Stocker, and M. Bleicher, *ibid.* **73**, 021901(R) (2006).

[12] M. Gaździcki, M. I. Gorenstein, and St. Mrówczyski, Phys. Lett. **B585**, 115 (2004); M. I. Gorenstein, M. Gaździcki, and O. S. Zozulya, *ibid.* **B585**, 237 (2004); M. Gaździcki, J. Phys. Conf. Ser. **27**, 154 (2005).

[13] H. Stöcker and W. Greiner, Phys. Rep. **137**, 277 (1986); J. Cleymans and H. Satz, Z. Phys. C **57**, 135 (1993); J. Sollfrank, M. Gaździcki, U. Heinz, and J. Rafelski, *ibid.* **61**, 659 (1994); G. D. Yen, M. I. Gorenstein, W. Greiner, and S. N. Yang, Phys. Rev. C **56**, 2210 (1997); F. Becattini, M. Gaździcki, and J. Solfrank, Eur. Phys. J. C **5**, 143 (1998); G. D. Yen and M. I. Gorenstein, Phys. Rev. C **59**, 2788 (1999); P. Braun-Munzinger, I. Heppe, and J. Stachel, Phys. Lett. **B465**, 15 (1999); P. Braun-Munzinger, D. Magestro, K. Redlich, and J. Stachel, *ibid.* **B518**, 41 (2001); F. Becattini, M. Gaździcki, A. Keränen, J. Manninen, and R. Stock, Phys. Rev. C **69**, 024905 (2004).

[14] P. Braun-Munzinger, K. Redlich, and J. Stachel, *Published in Quark Gluon Plasma 3*, edited by R. C. Hwa and X.-N. Wang (World Scientific, Singapore), Chap. 1, pp. 491–599.

[15] F. Becattini, Z. Phys. C **69**, 485 (1996); F. Becattini and U. Heinz, *ibid.* **76**, 269 (1997); F. Becattini and G. Passaleva, Eur. Phys. J. C **23**, 551 (2002).

[16] V. V. Begun, M. Gaździcki, M. I. Gorenstein, and O. S. Zozulya, Phys. Rev. C **70**, 034901 (2004); V. V. Begun, M. I. Gorenstein, and O. S. Zozulya, *ibid.* **72**, 014902 (2005); A. Keränen, F. Becattini, V. V. Begun, M. I. Gorenstein, and O. S. Zozulya, J. Phys. G **31**, S1095 (2005); F. Becattini, A. Keranen, L. Ferroni, and T. Gabbriellini, Phys. Rev. C **72**, 064904 (2005); V. V. Begun, M. I. Gorenstein, A. P. Kostyuk, and O. S. Zozulya, *ibid.* **71**, 054904 (2005); J. Cleymans, K. Redlich, and L. Turko, *ibid.* **71**, 047902 (2005); J. Cleymans, K. Redlich, and L. Turko, J. Phys. G **31**, 1421-1435 (2005); V. V. Begun, M. I. Gorenstein, A. P. Kostyuk, and O. S. Zozulya, *ibid.* **32**, 935 (2006); V. V. Begun and M. I. Gorenstein, Phys. Rev. C **73**, 054904 (2006).

[17] V. P. Konchakovski, S. Haussler, M. I. Gorenstein, E. L. Bratkovskaya, M. Bleicher, and H. Stöcker, Phys. Rev. C **73**, 034902 (2006).

[18] M. Gaździcki and M. I. Gorenstein, Phys. Lett. **B640**, 155 (2006).

[19] U. Katscher, D. H. Rischke, J. A. Maruhn, W. Greiner, I. N. Mishustin, and L. M. Satarov, Z. Phys. A **346**, 209 (1993); Yu. B. Ivanov, V. N. Russkikh, and V. D. Toneev, Phys. Rev. C **73**, 044904 (2006).

[20] M. Rybczynski *et al*. (NA49 Collaboration), J. Phys. Conf. Ser. **5**, 74 (2005); T. Anticic *et al*. (NA49 Collaboration), Phys. Rev. C **70**, 034902 (2004); P. Dinkelaker (NA49 Collaboration), J. Phys. G **31**, S1131 (2005).

[21] A. Bialas and W. Czyz, Acta Phys. Pol. B **36**, 905 (2005).

[22] C. Alt *et al*. (NA49 Collaboration), Phys. Rev. C **70**, 064903 (2004).

[23] S. Jeon and V. Koch, Phys. Rev. Lett. **85**, 2076 (2000).

[24] M. Asakawa, U. Heinz, and B. Muller, Phys. Rev. Lett. **85**, 2072 (2000).

[25] K. Adcox *et al*. (PHENIX Collaboration), Phys. Rev. Lett. **89**, 082301 (2002).

[26] J. Adams *et al*. (STAR Collaboration), Phys. Rev. C **68**, 044905 (2003).

[27] M. Gazdzicki and S. Mrowczynski, Z. Phys. C **54**, 127 (1992).

[28] M. Gazdzicki, Eur. Phys. J. C **8**, 131 (1999).

[29] S. Mrowczynski, Phys. Rev. C **66**, 024904 (2002).

[30] J. Zaranek, Phys. Rev. C **66**, 024905 (2002).